actuators

MDPI

Article

Experimental Assessment of Fractional-Order PDD$^{1/2}$ Control of a Brushless DC Motor with Inertial Load

Luca Bruzzone *, Pietro Fanghella and Mario Baggetta

Department of Mechanical, Energy, Management and Transportation Engineering, University of Genoa, 16145 Genoa, Italy; pietro.fanghella@unige.it (P.F.); mario.baggetta@unige.it (M.B.)
* Correspondence: luca.bruzzone@unige.it; Tel.: +39-010-335-2967

check for updates

Abstract: The application of Fractional Calculus to control mechatronic devices is a promising research area. The most common approach to Fractional-Order (FO) control design is the PI$^\lambda$D$^\mu$ scheme, which adopts integrals and derivatives of non-integer order λ and μ. A different possible approach is to add FO terms to the PID control, instead of replacing integer order terms; for example, in the PDD$^{1/2}$ scheme, the half-derivative term is added to the classical PD. In the present paper, by mainly focusing on the transitory behaviour, a comparison among PD, PD$^\mu$, and PDD$^{1/2}$ control schemes is carried out, with reference to a real-world mechatronic implementation: a position-controlled rotor actuated by a DC brushless motor. While using a general non-dimensional approach, the three control schemes are first compared by continuous-time simulations, and tuning criteria are outlined. Afterwards, the effects of the discrete-time digital implementation of the controllers are investigated by both simulation and experimental tests. The results show how PDD$^{1/2}$ is an effective and almost cost-free solution for improving the trajectory-tracking performance in position control of mechatronic devices, with limited computational burden and, consequently, easily implementable on most commercial motion control drives.

Keywords: fractional-order control; half-derivative; position control

1. Introduction

The generalization of the concept of derivative and integral to non-integer order (Fractional Calculus) dates back to the beginning of the theory of differential calculus: there are notes by Leibnitz regarding the calculation of the half-derivative (that is the derivative of order 1/2) [1]. In the last decades, the advances in the chaos theory revealed deep relationships with fractional differential and integrals, and this motivated a renewed interest in this research area. In the scientific literature, there is a wide variety of works regarding the applications of fractional derivatives and integrals in physics [2], chemistry [3], and biology [4].

Fractional Calculus is not only a powerful tool for modelling some physical phenomena, but it can also be used in engineering applications, such as electronics, signal processing, and bioengineering [5]. In particular, Fractional Calculus can be profitably applied in the area of control system design. Most control system algorithms are based on integer-order derivatives and integrals of the error; if the derivation/integration order is not integer, but fractional, there are additional parameters that can be tuned to improve the closed-loop system behavior.

The PI$^\lambda$D$^\mu$ scheme is the most common approach to Fractional-Order (FO) control design, which generalizes the PID scheme by adopting integrals and derivatives of non-integer order λ and μ [6]. Design techniques, optimization tools and practical implementations of PI$^\lambda$D$^\mu$ controllers are discussed in [7–14]. In particular, the FO derivative of the PD$^\mu$ can lead to performance improvements in the transient behavior with respect to the classical PD in many motion control applications [15–24].

Besides the PI$^\lambda$D$^\mu$–PD$^\mu$ scheme, in the scientific literature there are many other examples of extensions of control techniques based on Fractional Calculus; for instance, the performance of sliding mode control can be enhanced by using a FO disturbance observer [25] or by applying it to systems that are better approximated by FO models [26].

Another possible approach to FO control is to add FO terms to the classical PID scheme, instead of replacing the integer order terms; for example, in the PDD$^{1/2}$ scheme, the half-derivative term is added to the derivative term instead of replacing it as in the HPD$^\mu$ [27–32]. One immediate advantage of this approach is that the well-known PID/PD scheme can be maintained, while performance improvements, if needed, can be achieved with the only addition of the half-derivative term.

In [31] the PD, PD$^\mu$, and PDD$^{1/2}$ schemes are compared by simulation in the control of a second-order (inertial) system, analyzing the dynamic behavior of the closed-loop system in terms of settling time, rise time, overshoot, and settling energy. The integral action is not used, since the focus of the research is the transient behavior and not the steady-state accuracy. A non-dimensional approach is used for the sake of generality. The simulation results show that, while considering the case of step input and keeping constant the settling energy, the PDD$^{1/2}$ scheme has a better readiness than PD and PD$^\mu$ The main drawback is a limited increase of overshoot.

The present paper continues and deepens the comparison between PD, PD$^\mu$, and PDD$^{1/2}$, with the aim of an experimental validation of the benefits of the FO control approach in real working conditions, not limited to the step response. The main advancements and differences with respect to [31] are the following:

- after a more detailed discussion of their performances in terms of settling time, rise time, overshoot and settling energy: in case of step response, the three controllers are compared by simulation, while keeping the overshoot constant (Section 5);
- then, the comparison is extended to the response in case of trapezoidal speed law, which is commonly used as reference signal for finite displacements of mechatronic systems, again by adopting a non-dimensional approach (Section 6); and,
- finally, the effects of discrete-time digital implementation of the controller with finite sampling time and short memory effect, suitable for limited capacity microcontrollers, are investigated both by simulations and by experimental tests on a real-world mechatronic test-bench: a position-controlled rotor actuated by a DC brushless motor (Section 7).

The simulations and experimental results show good agreement for both continuous and discrete-time models of the controller. Moreover, FO controllers PD$^\mu$ and PDD$^{1/2}$ exhibit better performances, in both simulations and in experiments, than the classical PD scheme, with a limited increase of computational burden.

2. The Integro-Differential Operator: Definition and Numerical Computation

In Fractional Calculus, according to the Grünwald–Letnikov definition, being suitable for a robust discrete-time implementation [33], the continuous fractional differential operator for a function $x(t)$ can be defined as:

$$\frac{d^\alpha}{dt^\alpha}x(t) = \lim_{h\to 0}\frac{1}{h^\alpha}\sum_{k=0}^{\left[\frac{t-a}{h}\right]} (-1)^k \frac{\Gamma(\alpha+1)}{\Gamma(k+1)\Gamma(\alpha-k+1)}x(t-kh) \qquad (1)$$

where $\alpha \in \mathbb{R}^+$ is the order of differentiation, a and t are the fixed and variable limits, Γ is the Gamma function, h is the time increment, and $[y]$ is the integer part of y.

Equation (1) can be rewritten in terms of z-transfer notation to obtain a discrete-time digital implementation with finite sampling time T_s [34]:

$$\frac{d^\alpha}{dt^\alpha}x(t) \cong \frac{1}{T_s{}^\alpha}\left[\sum_{j=0}^{k} w_j^\alpha z^{-j}\right] \qquad (2)$$

where $k = [(t–a)/T_s]$ and:

$$w_0^\alpha = 1$$
$$w_j^\alpha = \left(1 - \frac{\alpha+1}{j}\right)w_{j-1}^\alpha , \; j= 1, \, 2, \, \ldots \tag{3}$$

For the calculation of (2), it is necessary to consider $k + 1$ previous values of x; from a practical point of view, for $t \gg a$ the number of addends becomes too large for real-time implementation on a digital controller; therefore, it is necessary to limit the number of steps on which the calculation of the fractional derivative is based, in order to have a computational burden compatible with the sampling time and the speed of the controller CPU. Accordingly, if, at each time step, there is a fixed number n of considered previous steps, with $n < k$, Equation (2) corresponds to the application of a nth order digital filter, with fixed memory length L given by the product of the sampling time and of the filter order:

$$L = nT_s \tag{4}$$

Fortunately, for large t the history of the function $x(t)$ near the start point of the differentiation process ($t = a$) becomes negligible on the basis of the so-called short-memory principle [35], which means that only taking into account the recent past of the function, in the interval $[t–L, t]$, does not yield relevant approximations in the discrete-time evaluation of the FO derivative.

3. Second-Order Linear System with Fractional-Order Control

There is a wide variety of closed-loop mechatronic systems in which friction is negligible, and the inertial effects can be suitably modelled by a second-order linear system. In the following a rotor with inertia J subject to the control output torque M will be considered (obviously, all the results and conclusions can be extended to a translating mass m subject to a control output force F).

The plant dynamics is expressed by the following differential equation:

$$J\frac{d^2}{dt^2}\theta = M(e_\theta) \tag{5}$$

where M is the control output, which is a function of the error $e_\theta = \theta_r—\theta$ (difference between the set-point angle and the current angle).

In the following, for closed-loop control (Figure 1), two possible FO control laws are considered and compared: PD^μ and $PDD^{1/2}$.
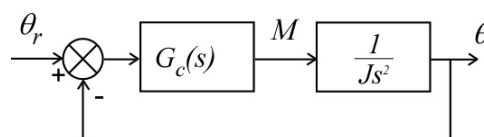

Figure 1. Closed-loop system with second-order plant.

In the case of PD^μ control, the control law is:

$$M(e_\theta) = K_p e_\theta + K_{fd}\frac{d^\mu}{dt^\mu}e_\theta \tag{6}$$

where K_p and K_{fd} are the proportional and fractional-order derivative gains and μ is the fractional derivative order.

In the case of $PDD^{1/2}$ scheme:

$$M(e_\theta) = K_p e_\theta + K_d\frac{d}{dt}e_\theta + K_{hd}\frac{d^{1/2}}{dt^{1/2}}e_\theta \tag{7}$$

where K_p, K_d, and K_{hd} are the proportional, derivative, and half-derivative gains.

If all of the derivatives of $x(t)$ are null at $t = 0$, the Laplace transform of FO derivatives has the same well-known property of integer-order derivatives [34]:

$$L\left[\frac{d^\alpha}{dt^\alpha}x(t)\right] = s^\alpha L[x(t)] \tag{8}$$

Therefore, the transfer functions of the PD^μ and $PDD^{1/2}$ controllers are:

$$G_{c,PD^\mu}(s) = K_p + K_{fd}s^\mu \tag{9}$$

$$G_{c,PDD^{1/2}}(s) = K_p + K_d s + K_{hd}s^{1/2} \tag{10}$$

4. Non-Dimensional Model

For the sake of generality, the system behaviour is analysed by using a dimensionless formulation. For the PD^μ control, besides the derivative order μ, the dimensionless parameter φ, proportional to K_{fd}, is introduced [31]:

$$\varphi = \frac{K_{fd}}{K_p}\omega_n^\mu = \frac{K_{fd}}{K_p^{(1-\mu/2)}J^{\mu/2}} \tag{11}$$

where $\omega_n = (K_p/J)^{1/2}$; for the $PDD^{1/2}$ control, two dimensionless parameters ζ and ψ, proportional to K_d and K_{hd}, are used [31]:

$$\zeta = \frac{K_d\omega_n}{2K_p} = \frac{K_d}{2\sqrt{K_pJ}} \tag{12}$$

$$\psi = \frac{K_{hd}}{K_p}\omega_n^{1/2} = \frac{K_{hd}}{K_p^{3/4}J^{1/4}} \tag{13}$$

The basic concept in the definition of these parameters is that the proportional effect acts as a torsional spring stiffness, therefore ω_n is the natural frequency of the undamped closed loop system. Consequently, Equation (12) corresponds to the well-known definition of damping ratio for a second-order linear system. The parameters φ and ψ have been defined to non-dimensionalize the gains K_{fd} and K_{hd} on the basis of K_p and ω_n, simply starting from dimensional analysis. The alternative expressions in Equations (11)–(13) derive from the expression of ω_n as a function of K_p and J.

From Equations (11)–(13) it is possible to recognize that:

- when $\mu = 1$ the PD^μ controller is a PD controller with $\zeta = \phi/2$; and,
- when $\mu = 1/2$ the PD^μ controller is a $PD^{1/2}$ controller with $\varphi = \psi$

To complete the non-dimensional approach, it is necessary to introduce also the dimensionless time $t_{ad} = \omega_n t$, the dimensionless position $\theta_{ad} = \theta/\theta_r$, and the dimensionless error $e_{\theta ad} = e_\theta/\theta_r$. Using these variables, and starting from Equations (5)–(7), it is possible to write the dimensionless dynamic equations of the closed-loop system with the two control laws:

$$PD^\mu: \frac{d^2}{dt_{ad}^2}\theta_{ad} = e_{\theta,ad} + \varphi\frac{d^\mu}{dt_{ad}^\mu}e_{\theta,ad} \tag{14}$$

$$PDD^{1/2}: \frac{d^2}{dt_{ad}^2}\theta_{ad} = e_{\theta,ad} + \psi\frac{d^{1/2}}{dt_{ad}^{1/2}}e_{\theta,ad} + 2\zeta\frac{d}{dt_{ad}}e_{\theta,ad} \tag{15}$$

Figure 2 presents the adoption of the dimensionless parameter and variables, where M_{ad} is the dimensionless torque, $\theta_{r,ad}$ is the dimensionless set-point, and $G_{c,ad}(s)$ is the dimensionless controller transfer function, which is in the two cases:

$$PD^\mu: G_{c,ad,PD^\mu}(s) = 1 + \varphi s^\mu \tag{16}$$

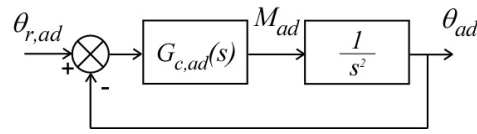$$\text{PDD}^{1/2}: G_{c,ad,PDD^{1/2}}(s) = 1 + \psi s^{1/2} + 2\zeta s \tag{17}$$

Figure 2. Dimensionless closed-loop system with second-order plant.

Starting from Equations (16) and (17), it is possible to obtain the dimensionless closed-loop transfer function of the system for the two control laws:

$$\text{PD}^{\mu}: \frac{\theta_{ad}}{\theta_{r,ad}} = G_{cl,ad,PD^{\mu}}(s) = \frac{1 + \varphi s^{\mu}}{1 + \varphi s^{\mu} + s^2} \tag{18}$$

$$\text{PDD}^{1/2}: \frac{\theta_{ad}}{\theta_{r,ad}} = G_{cl,ad,PDD^{1/2}}(s) = \frac{1 + \psi s^{1/2} + 2\zeta s}{1 + \psi s^{1/2} + 2\zeta s + s^2} \tag{19}$$

These dimensionless transfer functions depend only on two parameters: μ and φ for PD$^{\mu}$ control, ζ and ψ for PDD$^{1/2}$ control.

In the rest of this paper:

- PD, PD$^{\mu}$, and PDD$^{1/2}$ controls are compared non-dimensionally by simulation while considering the response to a step input (Section 5);
- the non-dimensional comparison by simulation is then extended to the response to a set-point with trapezoidal speed law, suitable for position control of mechatronic devices (Section 6); and,
- finally, the tuned PD, PD$^{\mu}$, and PDD$^{1/2}$ controllers are experimentally validated on a mechatronic test bench, with a discrete-time digital implementation that is suited to be executed by microcontrollers with limited computing power (Section 7).

5. Step Response

In this first analysis, simulations of system and controllers are performed in continuous time by using the FOTF Matlab library [34]. The system behaviour in the case of step-input can be evaluated considering these performance indexes:

- settling time to within 2% band;
- rise time from 10% to 90% of the final value;
- overshoot (%); and,
- dimensionless settling energy, being defined as follows [31]:

$$E_{s,ad} = \int_0^{\infty} M_{ad}^2 dt_{ad} \tag{20}$$

Figures 3–6 collect these indexes both in the case of PD$^{\mu}$ control, as a function of μ ($0 \div 2$), and φ ($0 \div 8$), and in the case of PDD$^{1/2}$ control, as a function of ζ ($0 \div 2$) and ψ ($0 \div 8$). These 3D graphs have been obtained varying the dimensionless parameters μ and ζ in steps of 0.01, and ψ and φ in steps of 0.05, generating 32000 simulations for PD$^{\mu}$ and 32000 simulations for PDD$^{1/2}$ control. The considered ranges of dimensionless parameters cover the useful zones for practical applications, as will be discussed in the following; moreover, since these 3D maps are based on dimensionless variables, they represent an exhaustive and general tool to compare PD, PD$^{\mu}$, and PDD$^{1/2}$ in the case of second-order plant and step set-point.
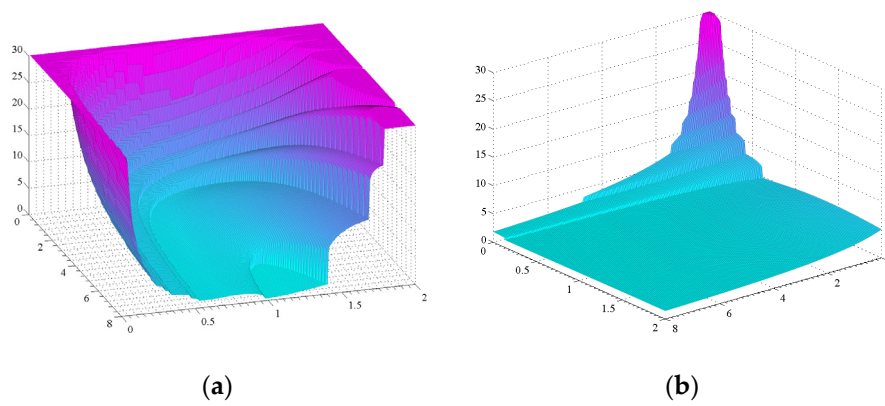
(**a**)   (**b**)

Figure 3. Dimensionless settling time with PD$^\mu$ control (**a**) and PDD$^{1/2}$ control (**b**).

(**a**)   (**b**)
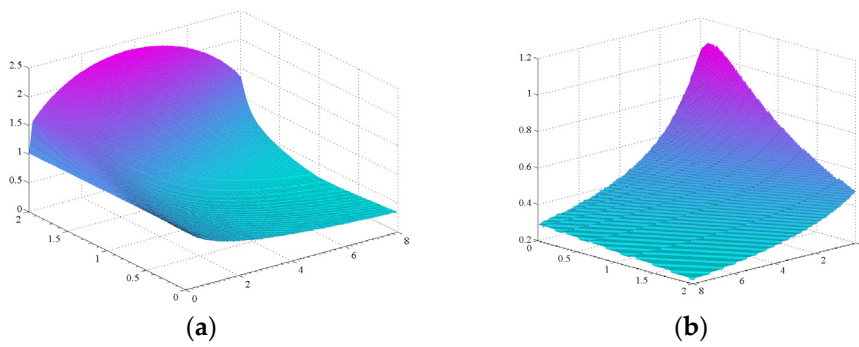
Figure 4. Dimensionless rise time with PD$^\mu$ control (**a**) and PDD$^{1/2}$ control (**b**).

(**a**)   (**b**)
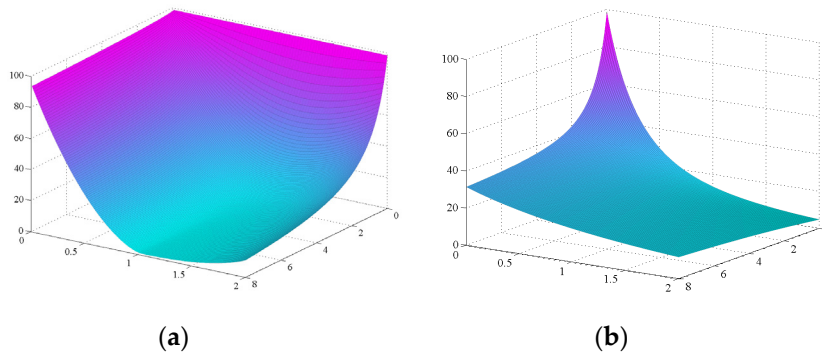
Figure 5. Overshoot (%) with PD$^\mu$ control (**a**) and PDD$^{1/2}$ control (**b**).

(**a**)   (**b**)
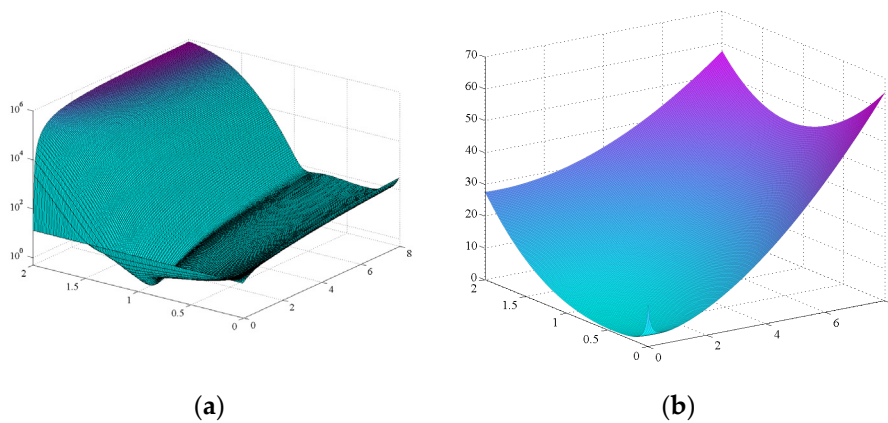
Figure 6. Dimensionless settling energy $E_{s,ad}$ with PD$^\mu$ control (**a**) and PDD$^{1/2}$ control (**b**).

It is possible to note that:

- the 3D surfaces representing the settling time are characterized by discontinuities, which are related to the number of oscillations, which are performed before reaching the 2% band; for the PD^μ control, the number of oscillations increases if φ tends to zero or if μ is distant from the unit value; for $PDD^{1/2}$ this number increases if both ζ and ψ tend to zero (absence of damping);
- overshoot is 100% without any damping ($\varphi = 0$ for PD^μ, $\zeta = \psi = 0$ for $PDD^{1/2}$); this graph can be used to impose a lower limit to the total damping: φ for PD^μ, the combination of ζ and ψ for $PDD^{1/2}$; and,
- for the PD^μ control, the three-dimensional (3D) graph of the settling energy show that the derivation order should range around the unit value, with an upper limit for φ; for $PDD^{1/2}$, this graph can be used to impose an upper limit to the total damping (the combination of ζ and ψ).

A practical method to use these 3D graphs is to single out the loci in the (μ, φ) and (ζ, ψ) planes characterized by constant value of one index (the contour lines of the corresponding 3D surface), and then assess the system behaviour along these loci.

For example, starting from the 3D graph of the overshoot for PD^μ, it is possible to obtain the five (μ, φ) loci with an overshoot equivalent to the PD with $\zeta = 0.6, 0.8, 1, 1.2, 1.4$ (Figure 7). Let us note that the integer order case (PD) is along the line with $\mu = 1$ and in this case $\zeta = \varphi/2$. Let us consider the central loci, with an overshoot equivalent to $PD_{1.0}$ (where the notation PD_x indicates PD with $\zeta = x$). Along this line, the five gain sets a', b', c', d', and e' have same overshoot (13.5%), and $\mu = 0.8, 0.9, 1, 1.1, 1.2$; therefore, c' corresponds to $PD_{1.0}$.
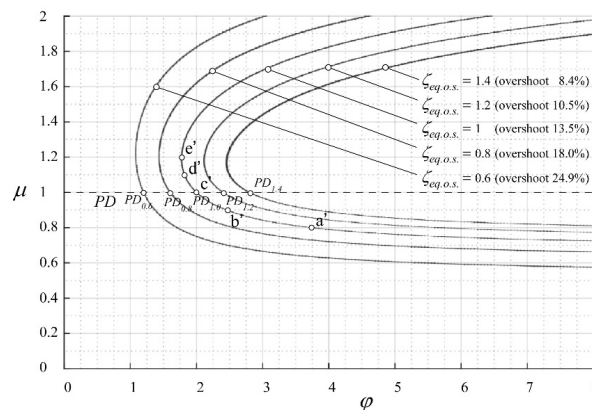

Figure 7. PD^μ control: (μ, φ) loci with equivalent overshoot.

Similarly, Figure 8 shows for $PDD^{1/2}$ the five (ζ, ψ) loci with overshoot equivalent to the PD with $\zeta = 0.6, 0.8, 1, 1.2,$ and 1.4. Along the central line, the five gain sets a'', b'', c'', d'', and e'' have the same overshoot (13.5%), and $\psi = 0, 0.5, 1, 1.5,$ and 2; therefore a'' corresponds to $PD_{1.0}$.

Figures 9 and 10 and Tables 1 and 2 summarize the step responses with these ten gain sets. It is possible to note that the $PDD^{1/2}$ scheme allows for reducing the settling and rise time with a lower increase of settling energy: for example, the gain set b'' has slightly better performance than b' with a remarkably lower settling energy.
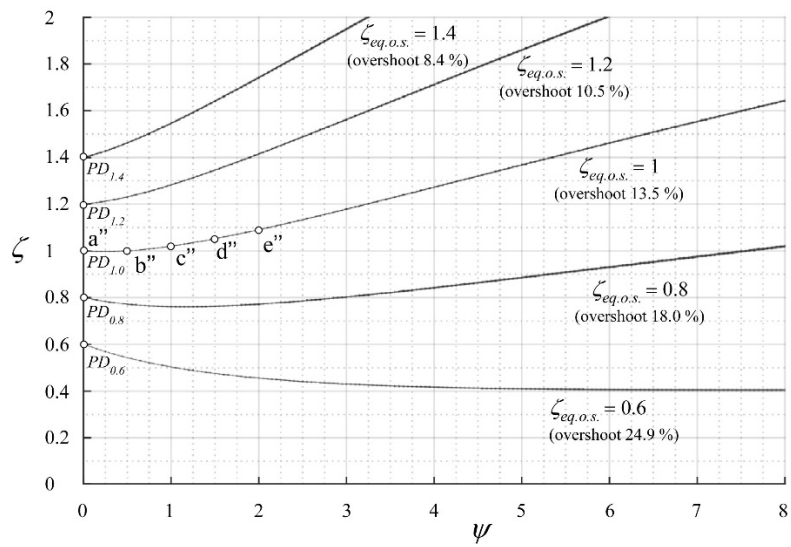
Figure 8. PDD$^{1/2}$ control: (ζ, ψ) loci with equivalent overshoot.
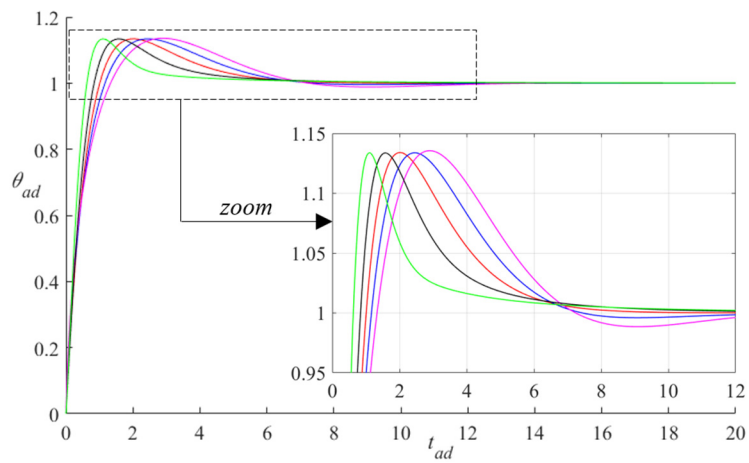

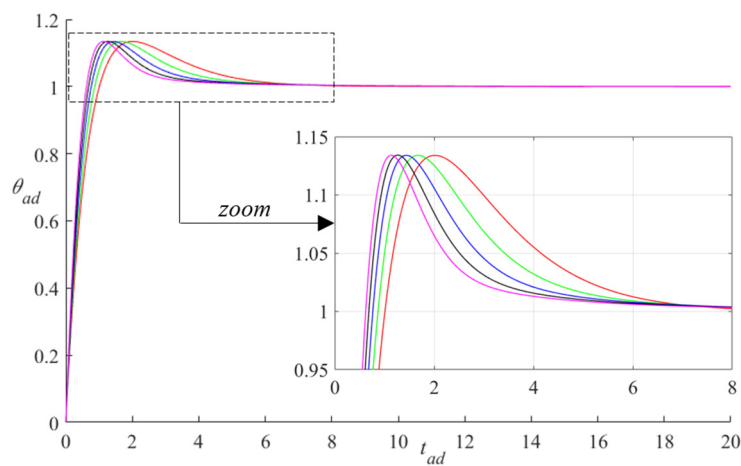**Figure 9.** Step response with PD$^\mu$ control: gain sets with equivalent overshoot (13.5%).

Figure 10. Step response with PDD$^{1/2}$ control: gain sets with equivalent overshoot (13.5%).

Table 1. PD/PD$^\mu$ comparison, μ–φ combinations with constant overshoot (13.5%).

Parameter Set	Colour in Figure 9	μ	φ	Dimensionless Settling Energy	Dimensionless Settling Time	Dimensionless Rise Time
a′ (PD$^\mu$)		0.8	3.75	17.84	3.46	0.46
b′ (PD$^\mu$)		0.9	2.46	5.28	4.78	0.62
c′ (PD, $\zeta = 1$)		1	2	3.14	5.41	0.73
d′ (PD$^\mu$)		1.1	1.82	22.60	5.87	0.84
e′ (PD$^\mu$)		1.2	1.76	137.28	6.28	0.95

Table 2. PD/PDD$^{1/2}$ comparison, ζ–ψ combinations with constant overshoot (13.5%).

Parameter Set	Colour in Figure 10	ζ	ψ	Dimensionless Settling Energy	Dimensionless Settling Time	Dimensionless Rise Time
a″ (PD, $\zeta = 1$)		1	0	3.14	5.41	0.73
b″ (PDD$^{1/2}$)		1	0.5	3.36	4.66	0.63
c″ (PDD$^{1/2}$)		1.02	1	4.08	4.07	0.57
d″ (PDD$^{1/2}$)		1.05	1.5	5.25	3.58	0.51
e″ (PDD$^{1/2}$)		1.09	2	6.83	3.19	0.46

The comparison among PD, PD$^\mu$, and PDD$^{1/2}$ with equivalent settling energy in the step response indicates that the PDD$^{1/2}$ control has a better readiness than the PD and PD$^\mu$ schemes, with the drawback of a limited increase of the overshoot; this comparison is extensively discussed in [31].

In the next section, the results that were obtained with step input will be extended to the more practical case of trapezoidal speed law, which is usually adopted to define the reference position in mechatronic applications; in particular, three control laws will be compared in continuous-time simulation:

- PD$_{1.0}$, gain set a″ of Table 2, equivalent to c′ of Table 1;
- PD$^\mu$, gain set a′ of Table 1, with $\mu = 0.8$ and $\varphi = 3.75$; and,
- PDD$^{1/2}$, gain set e″ of Table 2, with $\zeta = 1.09$ and $\psi = 2$.

These control laws have been tuned, imposing the constraint of equal overshoot in the step response (13.5%); a′ and e″ are the gain sets that have the lowest settling time and rise time in the respective tables.

6. Trapezoidal Speed Law Response

Finite displacements of mechatronic devices are never performed while using step inputs for the position set point, to avoid an instantaneous increase of the error and the consequential saturation of the control output. On the contrary, finite displacements are usually performed while adopting a trapezoidal speed law of the position set-point: a phase with constant acceleration, then a phase with constant speed, and finally a phase with constant deceleration. In the following, the response to this set-point law is analysed maintaining a non-dimensional approach for the sake of generality. To this aim, these assumptions are made:

- the total dimensionless rotation θ_{ad} has unit value; and,
- in the first and third phases, acceleration and deceleration are equal in magnitude, and consequently also the duration of these phases is equal; if the total dimensionless duration of the three phases is $t_{ad,fin}$, the duration of the first and third phases is $\alpha\, t_{ad,fin}$, with $0 < \alpha < 0.5$; consequently, the second phase duration is $(1–2\alpha)\, t_{ad,fin}$.

The first hypothesis is not restrictive, due to the model linearity; in practice, it corresponds to the assumption of unit step in the previous section. On the contrary, the second hypothesis

imposes a restriction, since, in general, the magnitudes of acceleration and deceleration can be different (for example, in many applications the deceleration rate is lower than the acceleration rate to obtain a more accurate final positioning). Nevertheless, these assumptions have been introduced to limit the number of combinations to be investigated, since the dimensionless trapezoidal speed law is completely defined by only two dimensionless parameters, $t_{ad,fin}$ and α. However, even with these assumptions, it is possible to obtain information about the system behaviour also in case of asymmetric speed laws, with different acceleration and deceleration by simply considering two responses with different values of α: as a matter of fact, the acceleration and deceleration transients are relatively independent for $\alpha << 0.5$ (sufficiently long constant speed phase), as usual in real applications.

As typical cases of the results that are obtained with trapezoidal laws, Figure 11 represents the response to trapezoidal speed law with $\alpha = 0.2$ and $t_{ad,fin} = 5$, in terms of dimensionless angle θ_{ad}, error $e_{\theta ad}$ and torque M_{ad}, while Figures 12 and 13 represent the same results, but with $t_{ad,fin} = 10$ and $t_{ad,fin} = 20$.
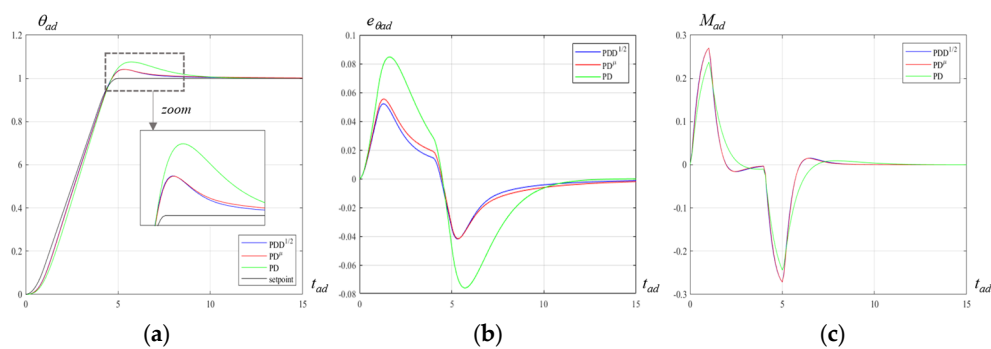

Figure 11. Trapezoidal speed law response, $\alpha = 0.2$, $t_{ad,fin} = 5$ (PD: green; PD$^\mu$: red; PDD$^{1/2}$: blue; set-point: black); dimensionless angle θ_{ad} (**a**), dimensionless error $e_{\theta ad}$ (**b**) and dimensionless torque M_{ad} (**c**).
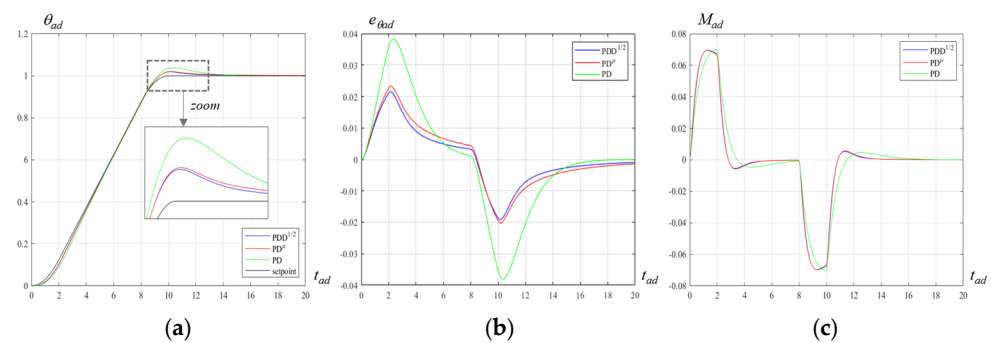

Figure 12. Trapezoidal speed law response, $\alpha = 0.2$, $t_{ad,fin} = 10$ (PD: green; PD$^\mu$: red; PDD$^{1/2}$: blue; set-point: black); dimensionless angle θ_{ad} (**a**), dimensionless error $e_{\theta ad}$ (**b**) and dimensionless torque M_{ad} (**c**).

Obviously, the tracking error decreases for higher values of $t_{ad,fin}$ with all three controllers, because the commanded motion is slower. It is possible to note that both the FO controllers show a better dynamic performance than the PD in terms of maximum tracking error: the peak error is remarkably reduced with a similar maximum value of the control torque M_{ad}. On the other hand, by using the classical PD controller, the tracking error decreases towards zero faster. The behaviours of PD$^\mu$ and PDD$^{1/2}$ controls are very close, even if the second has a slightly lower maximum error for all the displacement durations.

These results indicate that, also in the case of trapezoidal law, the adoption of FO controllers reduces the maximum tracking error. Interestingly, such a reduction is obtained without increasing the required motor torque, which remains very similar for all three control schemes.
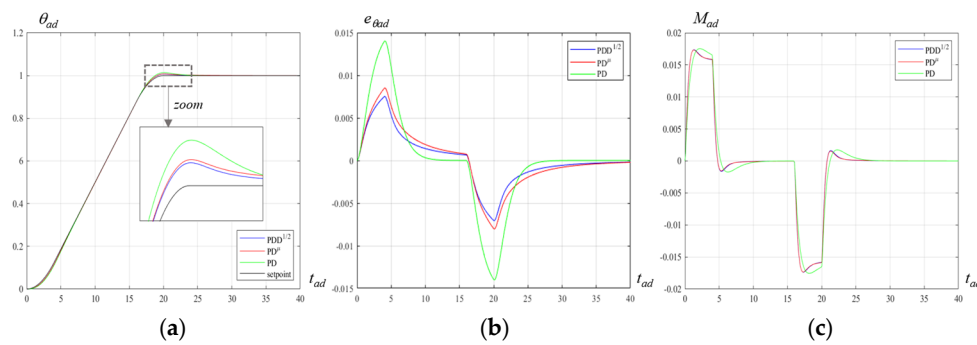
Figure 13. Trapezoidal speed law response, $\alpha = 0.2$, $t_{ad,fin} = 20$ (PD: green; PD^{μ}: red; $PDD^{1/2}$: blue; set-point: black); dimensionless angle θ_{ad} (**a**), dimensionless error $e_{\theta ad}$ (**b**) and dimensionless torque M_{ad} (**c**).

Until now, the simulations and obtained results are based on a continuous-time, non-approximated implementation of the fractional controllers, based, as already stated, on the FOTF toolbox [34]. In the case of real mechatronic systems, the control law must be implemented in discrete time by means of a digital filter, with finite memory length n, corresponding to the filter order due to the limited computation power available and real-time constraints (Section 2). Moreover, some non-modelled effects, such as friction, may arise, and their compensation may possibly be required.

In the next section, such topics will be investigated in two steps:

- by carrying out simulations with discrete-time, limited memory implementations of the controllers: in such a case, the control laws are implemented with sampling time T_s by digital filters with finite memory length n, with T_s, and n limited by the computational power of the controller hardware; and,
- by experimental tests on a physical prototype, to validate the possibility of obtaining the expected performance improvement also in real applications.

7. Discrete-Time Implementation and Experimental Validation

According to the previous considerations, the results of Section 6 have been validated, bearing in mind their application in real working environments, in two steps. First, the controllers have been implemented in discrete time and new simulations have been carried out and compared with the results of the previous sections. Subsequently, with the validated discrete-time implementation, the controllers have been tested and compared by means of an experimental set-up (Figure 14) composed of a flywheel (inertial load) directly connected to a DC motor Kollmorgen AKM42G (maximum continuous torque 3.4 Nm). The overall moment of inertia of the rotor (composed of motor rotor, joint, shaft, and flywheel) is 1.04×10^{-3} kgm^2.

Figure 15 represents the overall control scheme. The PD, PD^{μ}, and $PDD^{1/2}$ controls that are discussed in the previous section are implemented in Simulink Desktop Real Time running on a PC. A National Instrument PCI-6259 DAQ card, driven by Simulink Desktop Real Time, reads the encoder signal (position and velocity feedback) and generates the reference torque signal, which is sent to the Kollmorgen driver AKD-P00606. The no load torque/speed characteristics of the rotor (i.e., the torque necessary to drive the rotor at constant speed) has been measured and approximated by a linear characteristic with coefficient $K_f = 1.45 \times 10^{-3}$ Nms/rad to compensate for friction. Afterwards, a compensation torque proportional to the rotor speed with constant K_f has been added to the reference torque signal M_r (Figure 15) in all the three considered cases in order to obtain a coherent comparison: continuous-time simulation (CTS), discrete-time simulations (DTS), and experimental tests (ET).
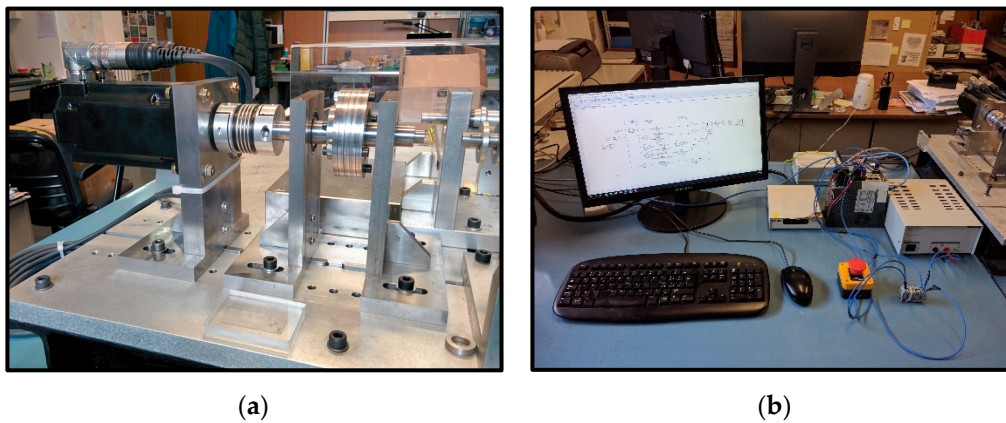
(**a**)   (**b**)

Figure 14. Experimental layout: inertial load directly actuated by the brushless DC motor (**a**) and Simulink Desktop Real Time control (**b**).
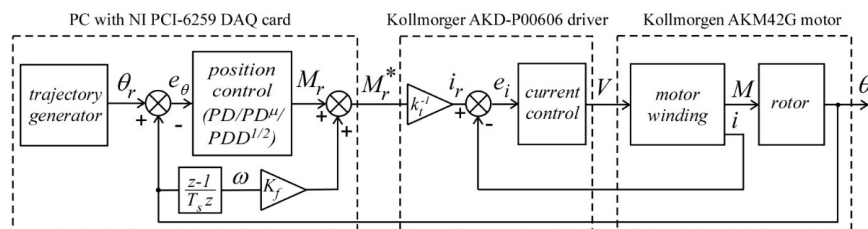

Figure 15. Overall control scheme of the experimental layout.

All of the tests have been performed while using a trapezoidal speed law with overall duration t_{fin} = 1 s and α = 0.2. The adopted proportional gain is K_p = 0.25 Nm/rad, therefore ω_n = 15.453 rad/s, and, consequently, $t_{ad,fin}$ = 15.453. Starting from the dimensionless parameters adopted for the comparison between PD, PD$^{\mu}$ and PDD$^{1/2}$ of the simulations reported in Section 6, the remaining control gains are calculated. Table 3 summarizes such gains and the other control parameters. For the discrete-time implementation of the controllers, the FO derivatives (half-derivative for PDD$^{1/2}$ and derivative of order μ for PD$^{\mu}$) are calculated by means of 6th order digital filters, according to the Grünwald–Letnikov approach, being expressed by Equations (2) and (3), adopting a sampling time T_s = 0.006 s. These values of filter order and sampling time are adequate to the computational capability of the control system.

Table 3. Experimental set-up and theoretical discrete-time simulation parameters.

	K_p [Nm/rad]	K_d [Nms/rad]	K_{hd} [Nms$^{1/2}$/rad]	K_{fd} [Nms$^{0.8}$/rad]	Total Rotation θ_r [rad]	Rotation Time t_{fin} [s]	Sample Time T_s [s]
PD		3.236×10^{-2}	-	-			
PDD$^{1/2}$	0.25	3.527×10^{-2}	0.127	-	80	1	0.006
PD$^{\mu}$		-	-	0.105			

Figure 16 shows the CTS results; differently from Section 6, these results are reported while using dimensional quantities (θ, e_θ and M) instead of dimensionless ones (θ_{ad}, $e_{\theta ad}$ and M_{ad}) to allow for the comparison with discrete-time control simulations and experimental results. Moreover, the torque graphs represent M^*_r (Figure 15), comprising the friction compensation term, which corresponds to the actual reference torque input to the AKD-P00606 motor driver.
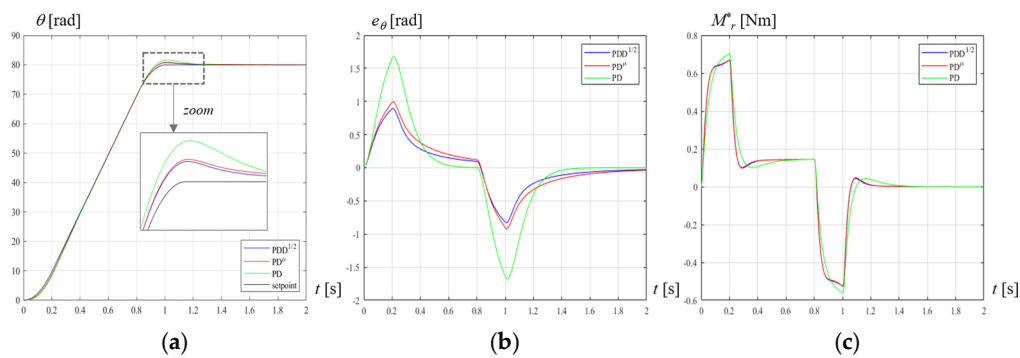
Figure 16. Trapezoidal speed law response, continuous-time simulation; $\alpha = 0.2$, $t_{fin} = 1$ s (PD: green; PD^μ: red; $PDD^{1/2}$: blue; set-point: black); angle θ (**a**), error e_θ (**b**) and torque M^*_r (**c**).

Discrete-time simulations (Figure 17), carried out by means of Simulink, allow for assessing the tracking performance of the FO controls with the fractional derivatives that were implemented by the 6th order digital filter. Finally, the same FO discrete-time implementation is adopted to control the motion of the experimental test bench of Figure 14, obtaining the results in Figures 18–20 provide detailed views of the acceleration and deceleration phases, comparing the results of CTS, DTS, and ET, while Table 4 summarizes the main quantitative results in terms of maximum and mean tracking error ($e_{\theta,max}$ and $e_{\theta,mean}$), maximum torque (M^*_{max}), and settling energy (E_s).
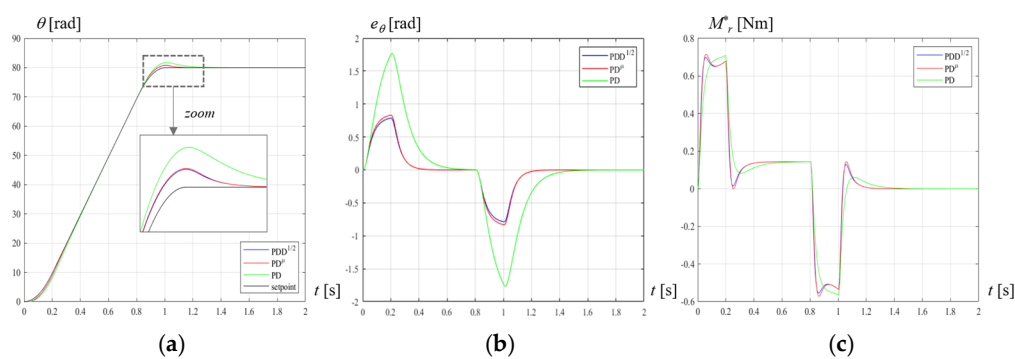

Figure 17. Trapezoidal speed law response, discrete-time simulation; $\alpha = 0.2$, $t_{fin} = 1$ s (PD: green; PD^μ: red; $PDD^{1/2}$: blue; set-point: black); angle θ (**a**), error e_θ (**b**) and torque M^*_r (**c**).
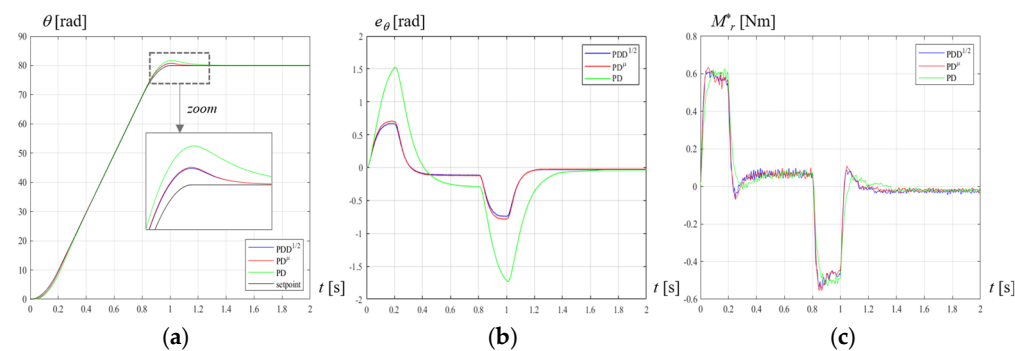

Figure 18. Trapezoidal speed law response, experimental test; $\alpha = 0.2$, $t_{fin} = 1$ s (PD: green; PD^μ: red; $PDD^{1/2}$: blue; set-point: black); angle θ (**a**), error e_θ (**b**) and torque M^*_r (**c**).
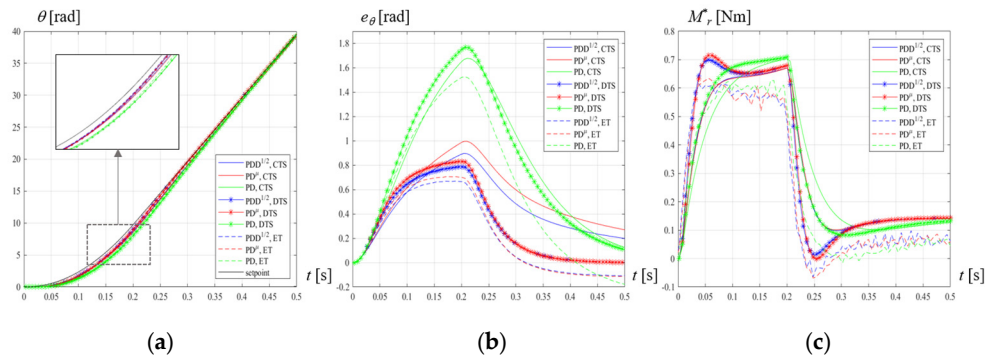
(a)　　　　　　　　　　　　　　(b)　　　　　　　　　　　　　　(c)

Figure 19. Trapezoidal speed law response, comparison of continuous-time simulation (CTS), discrete-time simulations (DTS), experimental tests (ET); $\alpha = 0.2$, $t_{fin} = 1$ s (PD: green; PD^{μ}: red; $PDD^{1/2}$: blue; set-point: black); zoom of the acceleration phase; angle θ (**a**), error e_{θ} (**b**) and torque M^{*}_{r} (**c**).
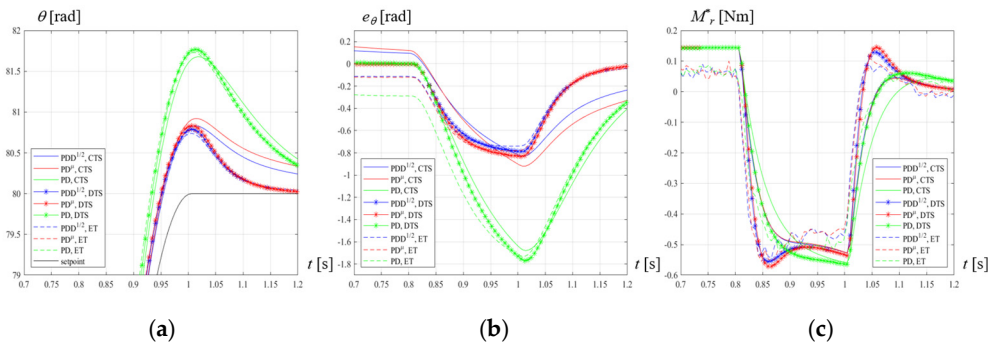

(a)　　　　　　　　　　　　　　(b)　　　　　　　　　　　　　　(c)

Figure 20. Trapezoidal speed law response, comparison of CTS, DTS, ET; $\alpha = 0.2$, $t_{fin} = 1$ s (PD: green; PD^{μ}: red; $PDD^{1/2}$: blue; set-point: black); zoom of the deceleration phase; angle θ (**a**), error e_{θ} (**b**) and torque M^{*}_{r} (**c**).

Table 4. Comparison of simulation results with PD, $PDD^{1/2}$, and PD^{μ}.

		$e_{\theta,\mathbf{max}}$ [rad]	$e_{\theta,\mathbf{mean}}$ [rad]	M^{*}_{max} [Nm]	E_s [N²m²s]
PD	CTS	1.679	0.624	0.704	22.016
	DTS	1.769	0.632	0.710	23.774
	ET	1.732	0.626	0.627	18.217
$PDD^{1/2}$	CTS	0.897	0.346	0.671	21.699
	DTS	0.789	0.279	0.699	24.201
	ET	0.741	0.296	0.616	18.319
PD^{μ}	CTS	0.997	0.386	0.670	21.631
	DTS	0.832	0.294	0.715	24.508
	ET	0.782	0.313	0.635	18.477

Starting from these results, we can draw the following conclusions:

- The simulated dynamics of the system with the discrete-time digital implementation of the FO controllers exhibits the same advantage with respect to the integer-order controller, which has been evidenced by the continuous-time model, as shown in Figures 16, 17 and 19: the peak tracking error is strongly reduced, and the improvement is even greater than in continuous time (−47% for $PDD^{1/2}$ and −41% for PD^{μ} in CTS, −55% for $PDD^{1/2}$, and −53% for PD^{μ} in DTS).

- The percentage decrease of the mean tracking error with respect to PD is similar to the decrease of the maximum tracking error: (−45% for $PDD^{1/2}$ and −38% for PD^{μ} in CTS, −56% for $PDD^{1/2}$, and −53% for PD^{μ} in DTS).

- On the other hand, the maximum peak torque is similar or even lower (−4.7% for PDD$^{1/2}$ and −4.8% for PD$^{\mu}$ in *C.T.S.*, −1.5% for PDD$^{1/2}$ and +0.7% for PD$^{\mu}$ in DTS); also the settling energies are similar (−1.4% for PDD$^{1/2}$ and −1.7% for PD$^{\mu}$ in *C.T.S.*, +1.8% for PDD$^{1/2}$ and +3.1% for PD$^{\mu}$ in DTS).

- Discrete-time simulation results and experimental data are in good agreement: the reduction of the peak tracking error with respect to PD is −57% for PDD$^{1/2}$ and −55% for PD$^{\mu}$; the reduction of the mean tracking error with respect to PD is −53% for PDD$^{1/2}$ and −50% for PD$^{\mu}$; the variation of maximum peak torque with respect to PD is −1.7% for PDD$^{1/2}$ and +1.3% for PD$^{\mu}$; and, the variation of settling energy with respect to PD is +0.6% for PDD$^{1/2}$ and +1.4% for PD$^{\mu}$.

- CTS and DTS both highlight the benefits of FO controllers and can be considered valuable tools for their tuning.

- The difference between PD$^{\mu}$ and PDD$^{1/2}$ is small, but, in the discrete-time implementation, PDD$^{1/2}$ exhibits slightly better performances, both in simulations and in experimental tests, since it provides slightly lower maximum and mean errors, with lower maximum torque and settling energy.

8. Conclusions

In the present paper, we highlight some of the benefits obtained by adopting FO motion controllers in mechatronic applications. The considered application is the position control of a rotor with constant inertia and actuated by a brushless motor, corresponding to quite a general case in motion control. In particular, the PDD$^{1/2}$ law is compared to the classical integer-order PD and the better-known FO PD$^{\mu}$ in the control of a second-order linear system.

First, while using a dimensionless approach, different possible tuning criteria based on the step response are discussed for PD, PD$^{\mu}$, and PDD$^{1/2}$ by means of simulations, and then a tuning criterium based on imposed overshoot value is adopted.

A digital implementation based on finite sampling time and finite memory length and a compensation of the friction losses are introduced, simulated, and implemented on an experimental workbench in order to compare the three controllers according to a real computational implementation and in experimental tests. Based on the tuning results for the step response, the controllers' performance has been tested with a trapezoidal speed law, a case that is more suited for real position control of mechatronic devices. The experimental results are coherent with the discrete-time simulations and confirm the efficacy of the proposed FO PDD$^{1/2}$ algorithm.

The work shows a practical demonstration that PDD$^{1/2}$ is an effective and almost cost-free solution to improve the trajectory-tracking performance in position control of mechatronic devices, with very limited computational burden (6th order digital filter) and, consequently, easily implementable on most commercial motion control drives.

As regards future works and challenges, there are several issues to be investigated. First, also integral terms will be added to the PDD$^{1/2}$ control algorithm in order to extend the proposed approach to applications in which the steady-state error must be bounded. The comparison between PID$^{\mu}$ and PII$^{1/2}$DD$^{1/2}$ (comprising the half-integral term) is currently in progress. Numerical optimization techniques that are based on the available and validated continuous-time and discrete-time models can be obviously applied, but it is even more interesting from a theoretical point of view the development of a general treatment in the frequency domain of the proposed control algorithms based on the half-derivative and half-integral terms.

Moreover, a fundamental and open problem for FO linear time invariant closed-loop systems is their robust stability, which is related to the preservation of the control properties in the presence of uncertainties of the controlled plant model [36–38]; also, this aspect will be considered in future research.

References

1. Miller, K.S.; Ross, B. *An Introduction to the Fractional Calculus and Fractional Differential Equations*; John Wiley & Sons: New York, NY, USA, 1993.
2. Hilfer, R. *Applications of Fractional Calculus in Physics*; World Scientific: Singapore, 2000.
3. Bard, A.J.; Faulkner, L.R. *Electrochemical Methods: Fundamentals and Applications*, 2nd ed.; John Wiley & Sons: New York, NY, USA, 2001.
4. Rihan, F.A. Numerical Modeling of Fractional-Order Biological Systems. *Abstr. Appl. Anal.* **2013**, *2013*, 816803. [CrossRef]
5. Gutiérrez, R.E.; Rosário, J.M.; Machado, J.T. Fractional Order Calculus: Basic Concepts and Engineering Applications. *Math. Probl. Eng.* **2010**, *2010*, 375858. [CrossRef]
6. Podlubny, I. Fractional-order systems and $PI^{\lambda}D^{\mu}$ controllers. *IEEE Trans. Autom. Control* **1999**, *44*, 208–213. [CrossRef]
7. Yeroglu, C.; Tan, N. Note on fractional-order proportional-integral-differential controller design. *IET Control Theory Appl.* **2012**, *5*, 1978–1989. [CrossRef]
8. Duma, R.; Dobra, P.; Trusca, M. Embedded application of fractional order control. *Electron. Lett.* **2012**, *48*, 1526–1528. [CrossRef]
9. Beschi, M.; Padula, F.; Visioli, A. The generalised isodamping approach for robust fractional PID controllers design. *Int. J. Control* **2015**, *90*, 1157–1164. [CrossRef]
10. Sondhi, S.; Hote, Y.V. Fractional order PID controller for perturbed load frequency control using Kharitonov's theorem. *Electr. Power Energy Syst.* **2016**, *78*, 884–896. [CrossRef]
11. Kesarkar, A.A.; Selvaganesan, N. Tuning of optimal fractional-order PID controller using an artificial bee colony algorithm. *Syst. Sci. Control Eng.* **2015**, *3*, 99–105. [CrossRef]
12. Khubalkar, S.; Chopade, A.; Junghare, A.; Aware, M.; Das, S. Design and Realization of Stand-Alone Digital Fractional Order PID Controller for Buck Converter Fed DC Motor. *Circuits Syst. Signal Process.* **2016**, *35*, 2189–2211. [CrossRef]
13. Saidi, B.; Amairi, M.; Najar, S.; Aoun, M. Bode shaping-based design methods of a fractional order PID controller for uncertain systems. *Nonlinear Dyn.* **2015**, *80*, 1817–1838. [CrossRef]
14. Anantachaisilp, P.; Lin, Z. Fractional Order PID Control of Rotor Suspension by Active Magnetic Bearings. *Actuators* **2017**, *6*, 4. [CrossRef]
15. Yang, J.; Dong, L.; Liao, X. Fractional order PD controller based on ADRC algorithm for DC motor. In Proceedings of the IEEE Transportation Electrification Conference and Expo, ITEC Asia-Pacific 2014, Beijing, China, 31 August–3 September 2014.
16. Jin, Y.; Luo, Y.; Wang, C.; Chen, Y.Q. LabView Based Experimental Validation of Fractional Order Motion Controllers. In Proceedings of the 2009 Chinese Control and Decision Conference, Guilin, China, 17–19 January 2009; pp. 323–328.
17. Dimeas, I.; Petras, I.; Psychalinos, C. New analog implementation technique for fractional-order controller: A DC motor control. *AEU Int. J. Electron. Commun.* **2017**, *78*, 192–200. [CrossRef]
18. Sun, G.; Ma, Z.; Yu, J. Discrete-Time Fractional Order Terminal Sliding Mode Tracking Control for Linear Motor. *IEEE Trans. Ind. Electron.* **2018**, *65*, 3386–3394. [CrossRef]
19. Haji, V.; Monje, C. Fractional-order PID control of a chopper-fed DC motor drive using a novel firefly algorithm with dynamic control mechanism. *Soft Comput.* **2018**, *22*, 6135–6146. [CrossRef]
20. Chen, S.Y.; Li, T.H.; Chang, C.H. Intelligent fractional-order backstepping control for an ironless linear synchronous motor with uncertain nonlinear dynamics. *ISA Trans.* **2019**, *89*, 218–232. [CrossRef] [PubMed]
21. Hekimoglu, B. Optimal Tuning of Fractional Order PID Controller for DC Motor Speed Control via Chaotic Atom Search Optimization Algorithm. *IEEE Access* **2019**, *7*, 38100–38114. [CrossRef]
22. Puangdownreong, D. Fractional order PID controller design for DC motor speed control system via flower pollination algorithm. *Trans. Electr. Eng. Electron. Commun.* **2019**, *17*, 14–23. [CrossRef]

23. Zheng, W.; Luo, Y.; Pi, Y.; Chen, Y. Improved frequency-domain design method for the fractional order proportional-integral-derivative controller optimal design: A case study of permanent magnet synchronous motor speed control. *IET Control Theory Appl.* **2018**, *12*, 2478–2487. [CrossRef]

24. Lino, P.; Maione, G. Cascade Fractional-Order PI Control of a Linear Positioning System. *IFAC PapersOnLine* **2018**, *51*, 557–562. [CrossRef]

25. Wang, Z.; Wang, X.; Xia, J.; Shen, H.; Meng, B. Adaptive sliding mode output tracking control based-FODOB for a class of uncertain fractional-order nonlinear time-delayed systems. *Sci. China Technol. Sci.* **2020**. [CrossRef]

26. Meng, B.; Wang, X.; Zhang, Z.; Wang, Z. Necessary and sufficient conditions for normalization and sliding mode control of singular fractional-order systems with uncertainties. *Sci. China Inf. Sci.* **2020**. [CrossRef]

27. Bruzzone, L.; Bozzini, G. Application of the $PDD^{1/2}$ algorithm to position control of serial robots. In Proceedings of the 28th IASTED International Conference Modelling, Identification and Control (MIC 2009), Innsbruck, Austria, 16–18 February 2009; pp. 225–230.

28. Bruzzone, L.; Bozzini, G. $PDD^{1/2}$ control of purely inertial systems: Nondimensional analysis of the ramp response. In Proceedings of the 30th IASTED International Conference Modelling, Identification, and Control (MIC 2011), Innsbruck, Austria, 14–16 February 2011; pp. 308–315.

29. Bruzzone, L.; Fanghella, P. Fractional order control of the 3-CPU parallel kinematics Machine. In Proceedings of the 32nd IASTED International Conference Modelling, Identification and Control (MIC 2013), Innsbruck, Austria, 11–13 February 2013; pp. 286–292.

30. Bruzzone, L.; Fanghella, P. Fractional-order control of a micrometric linear axis. *J. Control Sci. Eng.* **2013**, *2013*, 947428. [CrossRef]

31. Bruzzone, L.; Fanghella, P. Comparison of $PDD^{1/2}$ and PD^{μ} position controls of a second order linear system. In Proceedings of the 33rd IASTED International Conference on Modelling, Identification and Control (MIC 2014), Innsbruck, Austria, 17–19 February 2014; pp. 182–188.

32. Corinaldi, D.; Palpacelli, M.; Carbonari, L.; Bruzzone, L.; Palmieri, G. Experimental analysis of a fractional-order control applied to a second order linear system. In Proceedings of the 10th IEEE/ASME International Conference on Mechatronic and Embedded Systems and Applications (MESA 2014), Senigallia, Italy, 10–12 September 2014.

33. Machado, J.T. Fractional-order derivative approximations in discrete-time control systems. *J. Syst. Anal. Model. Simul.* **1999**, *34*, 419–434.

34. Xue, D. FOTF Toolbox for Fractional-Order Control Systems. In *Applications in Control*; Petráš, I., Ed.; De Gruyter: Berlin, Germany; Boston, MA, USA, 2019; pp. 237–266.

35. Das, S. *Functional Fractional Calculus*; Springer: Berlin/Heidelberg, Germany, 2011.

36. Matusu, R.; Senol, B.; Pekar, L. Robust stability of Fractional-Order Linear Time-Invariant systems: Parametric versus unstructured uncertainty models. *Complexity* **2018**, *2018*, 8073481. [CrossRef]

37. Lu, J.-G.; Chen, G. Robust stability and stabilization of Fractional-Order interval systems: An LMI approach. *IEEE Trans. Autom. Control* **2009**, *54*, 1294–1298.

38. Mohsenipour, R.; Jegarkandi, M.F. Robust stability analysis of fractional-order interval systems with multiple time delays. *Int. J. Robust Nonlinear Control* **2019**, *29*, 1823–1839. [CrossRef]